8

Research Article

Mohammad Amiri*, Marzieh Aryanpour, and Fatemeh Porhonar

Microstructural study of concrete performance after exposure to elevated temperatures via considering C-S-H nanostructure changes

https://doi.org/10.1515/htmp-2022-0030 received June 11, 2021; accepted March 10, 2022

Abstract: Evaluation of the concrete behavior in elevated temperatures is important in terms of first, structural construction safety under specified loadings, and second, measuring the loading capacity to continue operation. Furthermore, concrete behavior at high temperatures is strongly affected by microstructure. The calcium silicate hydrate (C-S-H), a nanostructure which is produced by hydration of cement paste, plays a significant role in enhancing the concrete strength under the impression of thermal fluctuations. Hence, this study investigates the microstructural performance of concrete exposed to high temperatures with a special focus on C-S-H nanostructure. Accordingly, 300 samples were cured for 1, 3, 7, 14, and 28 days in a moist room and then exposed to temperature range of 25-900°C for 2h to investigate changes in their weight, length, compressive strength, and cracking behavior. Besides evaluating the microstructural behavior of the specimens in different temperatures, several techniques such as SEM, EDX, and XRD have been employed. Based on the results, any changes in the samples' length, weight, and compressive strength depend on the C-S-H nanostructure behavior. In fact, following water decomposition from the C-S-H nanostructure at 900°C, the structure is partially converted to porous ceramic. These structural changes have caused a decline of 79–100% of the compressive strength. The compressive strength has decreased from 27.6 MPa to about 6 MPa. Also, the weight loss percentage of 28-days-old

sample at this temperature was 18.84%. Based on the SEM

and XRD results, this decline under high temperature arises

1 Introduction

The resistance of the construction against high temperature is one of the main factors of building grading in its fire tolerance and protection [1–4]. Furthermore, the fire resistance of concrete is dependent on many factors, including position and number of the heated compartments, fire type, boundary condition, spalling, and cracks [5,6].

The intensity of destruction in the fire is due to the amount of heat released during the fire. Part of this heat is spread in the firing atmosphere, while the rest is absorbed by building materials and members. Thus, the structural species lose their mechanical resistance and get degraded or seriously damaged at a critical temperature [7,8]. In fact, concrete is more commonly used in buildings due to its low electrical conductivity, specific heat, and the potential to withstand high fire temperatures. However, it does not mean that high temperature does not affect concrete. To illustrate, when the concrete is exposed to high temperature, its mechanical properties, including compressive strength, modulus of elasticity, and stability, are reduced dramatically. Therefore, the properties of concrete retained after the fire are important in measuring load capacity and structural reconstruction [9,10]. The extent of fire damage is directly related to the fire's duration and the resulting temperature [11]. However, cement concrete has good fire resistance for normal applications, its compressive strength changes at high temperatures due to extensive physical and chemical changes [12-14].

Fatemeh Porhonar: Faculty of Engineering, Department of Civil Engineering, University of Hormozgan, Bandar Abbas, Iran ORCID: Mohammad Amiri 0000-0002-3751-0261

Bandar Abbas, Iran

due to the collapse of C–S–H nanostructure and formation of calcium oxide in the cement structure. **Keywords:** high temperatures, concrete, compressive strength, C–S–H, SEM, XRD

^{*} Corresponding author: Mohammad Amiri, Faculty of Engineering, Department of Civil Engineering, University of Hormozgan, Bandar Abbas, Iran, e-mail: amirii@hormozgan.ac.ir

Marzieh Aryanpour: Faculty of Engineering, Department of Civil Engineering, Islamic Azad University of Bandar Abbas,

The deterioration of concrete exposed to high temperatures is attributed to the thermal mismatch due to the expansion of siliceous aggregate and shrinkage of cement paste matrix [15,16], the decomposition of hydrates due to the decomposition of Portlandite (CH) and C–S–H (calcium–silicate–hydrate) [17], the coarsening of pore structure due to void formation as a result of loss of bound water [18], and cracking that develops as a result of the rehydration of lime [19].

Furthermore, the chemical composition and physical structure of concrete exposed to high temperatures vary considerably. When the fire is extinguished by water, Ca(OH)₂ (one of the essential constituents in cement mortar) is converted to CaO, leading to the cracking and destruction of the concrete [20]. High temperatures influence the shape of the surface cracking and concrete scaling [1]. The cement matrix study results show that the reaction of cement phases with water results in the production of C-S-H nanostructures [21]. These structures account for about 70% of the volume of fully hydrated cement paste solids. The most important effect of hydration is in determining the mechanical and strength properties of the concrete [22]. The reason for showing this compound in the form of C-S-H is that its components' exact ratio is unknown. The C/S ratio and water are variables as well. During the formation process, the C-S-H nanostructures are initially like weak fiber crystals, whereas on the completion of hydration process, it gradually turns to a cohesive mass [22-24].

Several models have been proposed to describe the exact C–S–H structure [23,25]. According to the Powers-Brunauer model, this structure is a layer with a large area. The surface area of C–S–H was suggested to be around 100–700 m²/g. This structure's strength is attributed to the van der Waals forces [25,26]. In the Feldman-Sereda model, C–S–H's structure is a series of irregular layers arranged randomly, forming interlayer spaces of various sizes and shapes with dimensions of 5–25 Å [27,28]. Research works on Portland cement structure show that the C–S–H nanostructure is the cause of the cement mortar strength, although this structure changes at high temperatures.

Hertz [9] reported that the C-S-H structure decomposed at 600°C and degraded at 800°C. It also melted at temperatures above 1,150°C. Other minerals in the cement have also been converted to crystals, resulting in drastic microstructural changes, which reduce concrete strength and durability. Topcu and Demir [29] found that cement mortars lose their bonding properties due to water evaporation from the C-S-H nanostructure.

Arioz [30] observed that samples exposed to 400°C did not undergo significant surface changes. As the temperature rises to 600°C, the concrete begins to break, but its effect on the concrete surface is not significant. Concrete starts cracking at 800°C; hence, as the temperature rises to 1,000°C, these cracks increase. After being exposed to 1,200°C, the samples were completely decomposed and lost their bonding properties due to excessive cracking. According to the previous studies [31–33], the type and properties of the aggregates play an essential role in thermally-affected concrete behavior. The compressive strength of concrete with different aggregates at high temperatures is not the same. This is related to the structure of the concrete minerals. The quartz changes at 570°C with increasing volume and the damage is derived. Chen et al. studied the damage evaluation and pore structure of 10-year-old concrete cores after exposure to high temperatures. Based on the nonlinear resonance vibration theory, the nonlinear resonance frequency varied when the impact energy changed, and the degree of variation was directly related to the damage. In the study, the measured damages at the temperature of 20, 200, 400, and 600°C were 0, 0.57, 0.89, and 0.95, respectively. After exposure to different high temperatures, microscopic characteristics of old concrete, such as the total porosity, pore size distribution, the critical pore radius, and the threshold pore radius, were studied based on mercury intrusion porosimetry. It was found that the total porosity, critical pore radius, and threshold pore radius increased with the increase in the temperature [34].

Berenjian et al. [35] investigated the effect of high temperature on self-compacting concrete properties containing powder additives. They concluded that 20% metakaolinite and fly ash caused increase in the compressive strength at ambient temperatures. Also, increase in the temperature from 20 to 700°C reduces the compressive strength of control sample and pozzolan (zeolite, silica fume, metakaolinite, and fly ash) containing samples by about 11 and 8%, respectively. Compared to the control sample, in pozzolan-containing specimens, the ultrasonic velocity drop decreased with increase in the temperature.

Although the effect of temperature on concrete strength has been studied extensively, this process has not been investigated from a microstructural perspective in terms of C–S–H nanostructural changes and their impact on the compressive strength of the concrete. Therefore, the present study aimed to investigate the behavioral changes in C–S–H nanostructures and the formation of new compounds under the influence of temperature and their role in concrete's mechanical and strength parameters.

Table 1: Physical characteristics and chemical compositions of Portland cement II

Materials	Physical characteristics		Chemical compositions (%)							
	Specific gravity	Blaine fineness (cm ² /g)	SiO ₂	Al ₂ O ₃	Fe ₂ O ₃	CaO	MgO	K ₂ O	Na ₂ O	Loss on ignition
Cement II	3.14	3,400	21.50	5.30	3.00	64.00	2.50	0.70	1.50	1.50

2 Materials and methods

All the samples were made of Portland cement type 2 from Hormozgan. Most of the experiments performed in this study are based on the ASTM standard. The compressive strength test of the specimens was performed by a mechanical jack of "Azmoon Co." at a speed of 0.75 MPa/s. The chemical compositions of Portland cement were determined by X-ray fluorescence (XRF) analyses which are tabulated in Table 1.

Generally, the aggregates with a continuous grading curve yield the most satisfactory results. Therefore, grading for fine (sand) and coarse (gravel) particles was performed by ASTM C136-96 and ASTM C136 standards, respectively [36].

The grading curve of the coarse and fine aggregates is shown in Figure 1. The gravel and sand water absorption was obtained as 0.16 and 1.03% (ASTM C566-97 [37] and ASTM C127-88 [38]), respectively. In this study, the maximum diameter of aggregates used was 9.5 mm, and the

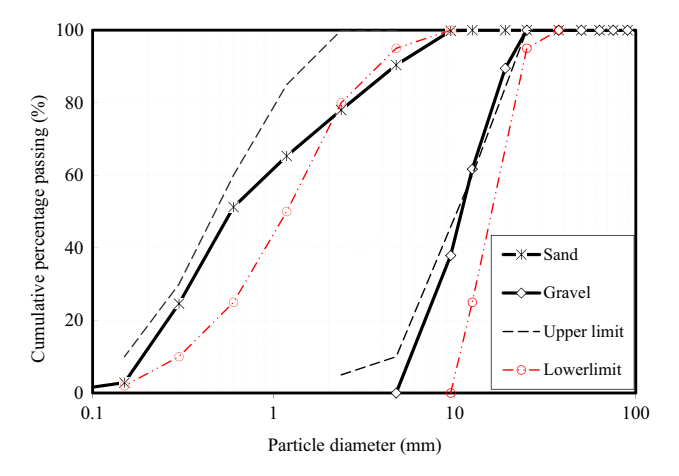


Figure 1: Grading curve of used materials (gravel and sand).

water used in making concrete was Hormozgan drinking water with pH = 7.8.

In concrete design with Portland cement, the used concrete slump was about $8-10\,\mathrm{cm}$ (ASTM C143 [39]). The specific gravity of cement concrete was considered as $2,345\,\mathrm{kg/m^3}$. The mixing pattern of the prepared samples is presented in Table 2.

Concrete production was conducted according to the ASTM C192/192M-2 standard [40]. The cement is first blended with the coarse and fine-grained sands in the mixer for 30 s. Then, the water was added to dry compounds, and stirring was continued for 2 min. The fresh mixture was poured into pre-prepared molds. Cube molds with dimensions of $50 \times 50 \times 50$ and $100 \times 100 \times 100$ mm were used to make concrete samples for the compressive strength test. According to the ASTM C31 standard, concrete made in 3 layers was poured into the mold with 25 blows (for compaction).

Results show that exposure to elevated temperatures affects larger specimens more adversely. As observed in the small specimens, the strength gain phenomenon after temperature exposure was no longer evident in the larger cast specimens. Heat conduction decreases significantly as specimen size increases. Therefore, there is a more significant difference in thermal gradient between the hotter exterior and cooler interior of these larger specimens. Thermal gradients increase with the increase in specimen size, resulting in thermal cracking [41]. Therefore, in this article, a compressive strength test was performed on Cubes of $50 \times 50 \times 50$ mm specimens (ASTM C109/C109M [42]) and $100 \times 100 \times 100$ mm specimens (ASTM C31 [43]) were cast using prepared concrete mixtures and cured in water for 1, 3, 7, 14, 28, and 90 days.

Afterward, the samples were air-dried in the laboratory for 1 day and oven-dried at 100°C for 24 h. Finally, the specimens were subjected to elevated temperatures (with 5°C/min heating rate) ranging from 100 to 900°C for 2 h.

Table 2: The mixing pattern of concrete with Portland cement II

Constituents	Cement (kg/m³)	Water (kg/m³)	Water/Cement	Gravel (kg/m³)	Sand (kg/m ³)
Cement	379.62	171	0.45	960	800

Then, the specimens were allowed to cool at a rate of 5°C/min and stored in a dry condition at room temperature for 2h before the experiments. A series of tests for measurement of weight loss (ASTM C1792-14 [44]), length changes (ASTM C157/C157M-17 [45]), and compressive strength variations (ASTM C39 [46]) were performed on the samples. Weight and length changes in the specimens were measured in two stages (pre-heat and post-heat) by digital scales and calipers, respectively. Then, all the specimens were placed under the concrete breaker mechanical jack to test the compressive strength (speed of 75 kg-f/s). It is worth mentioning that all experiments were repeated 3-5 times. Finally, the powder obtained from the samples was collected for microstructural examination using energydispersive X-ray analysis (EDX), scanning electron microscopy (SEM), and X-ray diffraction spectroscopy (XRD) via TESCAN-Vega3 and D8-advance apparatuses, respectively.

Furthermore, a D8 Advance Diffractometer from Bruker Company with Cu-K α radiation (λ = 1.54 Å) was used to determine the existing minerals in the concrete sample and collect the XRD pattern of concrete mineral fraction after heating. XRD analysis was carried out based on the method suggested in refs [47,48]. SEM TESCAN-Vega3 examined the microstructure and morphology of the compacted concrete samples after drying the samples under air and a gold coating of the specimen surface.

3 Results and discussion

3.1 Investigation of XRD of heat-exposed samples

XRD spectroscopy was used to determine the effect of temperature on the samples and the characterization of different composing elements. For this purpose, 28-days-old powder of cement samples heated at 25, 500, and 900°C was used to determine the concrete's crystalline structure. The pattern of peaks in Figure 2 shows the formed constituents, which are the predicator of strong cement hydration interaction and the formation of hydrated products.

The results of XRD spectroscopy in Figure 2 reveal the crystal structures and nanostructures of the hydrated calcium silicate (C–S–H). The C–S–H nanostructure has been composed of many small globules with irregular and disordered layered structure. Thus, it is a little difficult to detect it in the XRD pattern. C–S–H nanostructure consists of the hydration of calcium-containing compounds in

cement, including alite (C_3S) and belite (C_2S) , and is the main part of the hydration product of cement [49,50].

Crystalline phases, including quartz (at 3.5, 2.2, 1.9, and 1.8 Å), calcite (Ca) (at 3.8, 2.4, 1.9, and 1.6 Å), and hydrated phases including Portlandite (Ca(OH)₂) and ettringite (AFt¹) (at 10.0 and 1.6 Å), for concrete samples at temperature 25° C are discernable separately

Phase change in cementitious compounds, principally C-S-H, depends on the Ca/SiO₂ ratio, temperature, and the amount of pressure applied. The amount of water in C-S-H phase has a significant effect on the mechanical properties of concrete, and dehydration of C-S-H is associated with increased porosity in the samples [51]. Dehydration of C-S-H at 200°C takes place by evaporation of water from the surface pores of this nanostructure and at a more intense rate at 400°C. Consequently, the intensity of the peaks such as this nanostructure has been reduced at 500°C and eliminated at 900°C. Based on the results, the main peak of the C-S-H nanostructure (3.02 Å) is equal to 512 CpS. With an increase in temperature to 500°C, it experiences a sharp drop of 27% and has been finally eliminated at a temperature of 900°C. This trend is also present for other peaks of C-S-H nanostructures, which were completely removed at 900°C at intervals of 4.2, 3.3, 2.8, 2.0, and 1.8 Å. It does not form again due to heat application.

In the temperature range of 600° C, C–S–H degradation consists of alite (C_3 S) and belite (C_2 S) cement compounds. With increase in the temperature to 900° C, β -wollastonite (β -W) has been formed. It is worth mentioning that the phases formed due to the destruction of C–S–H are intensely affected by the C/S ratio so that by increasing the C/S ratio along with β -W, more belite values are formed. In fact, by increasing the C/S ratio, more C–S–H nanostructures are destroyed due to two reasons: irregular increase in C–S–H structure and collapse of cementitious compounds due to dehydration [52].

Calcite peak is observed at a 3.8 Å with an intensity of 82 CpS. With increase in temperature to 500°C, the intensity of the calcite peak decreases by 47% (43 CpS). This decrease in process continued until 900°C, and the calcite peak was eliminated at this temperature. Likewise, other peaks of the calcite mineral have been completely eliminated at 900°C [53]. According to researchers, calcite decomposes completely at a temperature of about 850°C. Decomposition of calcium carbonate (Ca(CO₃))

¹ Alumina ferric oxide tri-sulfate.

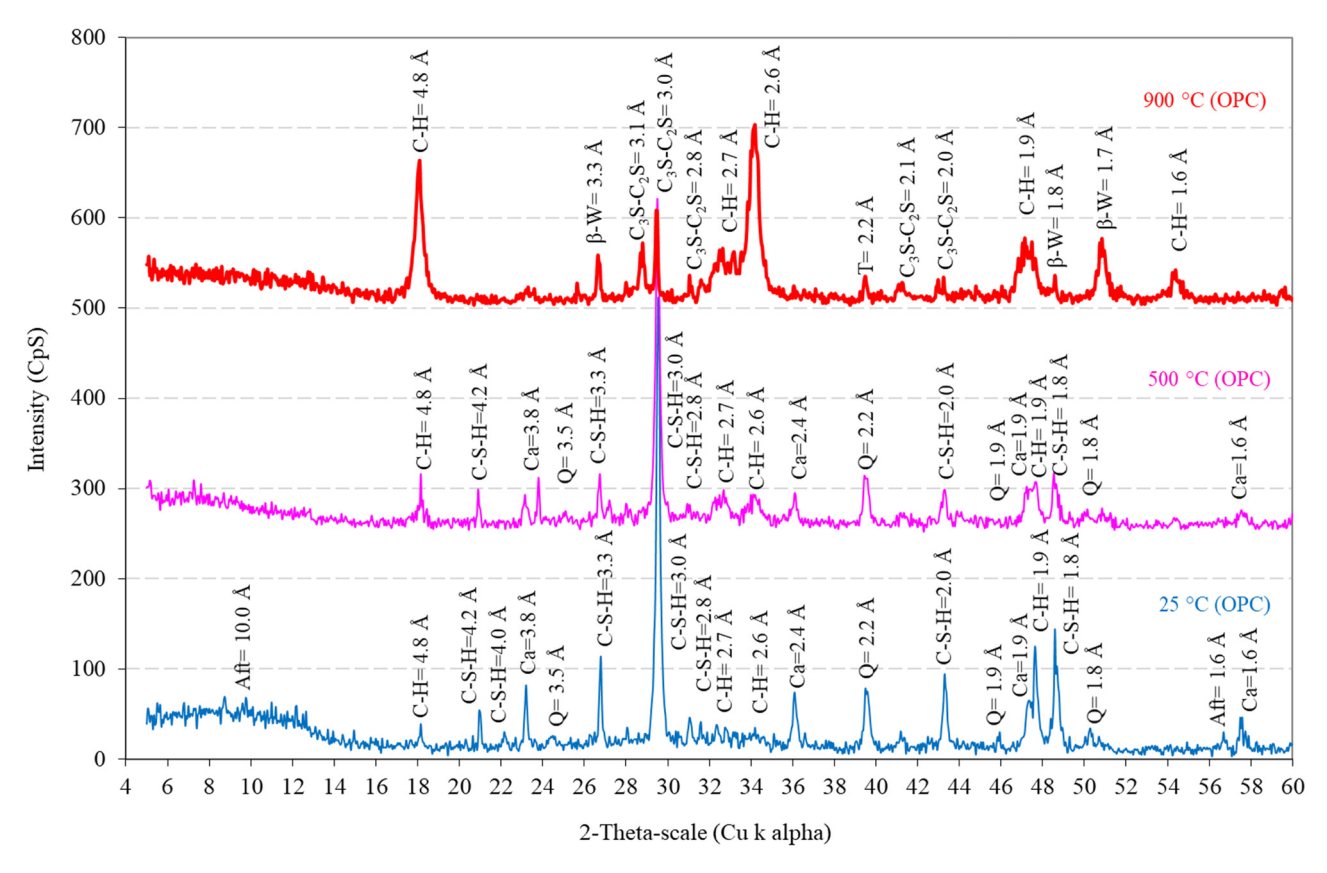


Figure 2: X-ray diffraction patterns of samples at temperatures of 25, 500, and 900°C. (AFt: ettringite, C_3S : alite, C_2S : belite, C-S-H: calcium silicate hydrate, CH: Portlandite, Q: quartz, Ca: calcite, β-W: β-wollastonite, T: tridymite).

due to heat, with the release of carbon dioxide (CO₂) gas, is converted to calcium oxide or quicklime (CaO).

Portlandite is another dominant product of the cement hydration process. The magnitude of the largest peak of Portlandite (1.9 Å) is 125 CpS. As the temperature rises to 500°C, its intensity decreases. Portlandite is dehydrated in the temperature range of 450–550°C and converted to quicklime and water (equation (1)) [54].

$$Ca(OH)_2 \rightarrow CaO + H_2O.$$
 (1)

Based on the X-ray diffraction pattern, with a decrease in Portlandite values at 500°C, a strong increase in Portlandite values is observed at a temperature of 900°C. Portlandite is known as the dominant phase at 900°C, so that it is observed in the distances of 4.8, 2.7, 2.6, 1.9, and 1.6 Å with intensities of 163 CpS, 66 Cps, 203 CpS, 77 CpS, and 42 CpS, respectively. Primary Portlandite is completely degraded at 550°C, and water released at 600°C due to dehydration of Portlandite in reaction with the released lime (due to decomposition of calcium carbonate and primary Portlandite) has led to the formation of secondary Portlandite. As the temperature increases, the amount of secondary Portlandite increases, which is clearly visible in

the XRD pattern. Due to formation in critical conditions, secondary Portlandite is dehydrated at a lower temperature than primary Portlandite. It has increased the volume of the concrete, increased cracks, and decreased the compressive strength of the concrete [50,54].

From the degradation of C–S–H at a temperature of 600°C, the compounds C_3S and C_2S of calcium silicates are formed. As the temperature increases, the amount of C_3S and C_2S increases so that at 900°C, the new peaks of C_3S and C_2S at intervals of 3.1, 3.0, 2.8, 2.1, and 2.0 Å has been formed at intensities of 72 CpS, 108 CpS, 36 CpS, 28 CpS, and 34 CpS [51,55]. Due to heat, it is not easy to distinguish between the formed alite and belite, and C_3S or C_2S peaks can be used to indicate both.

At 900°C, new peaks of β -We were formed at intervals of 3.3, 1.8, and 1.7 Å with intensities of 58 CpS, 36 CpS, and 77 CpS. After C–S–H degradation, in addition to alite and belite, β -W is formed in the temperature range of 800°C. It is worth noting that with increase in the C/S ratio, more β -W is formed [50].

The peaks of the needle-shaped mineral ettringite can be seen at intervals of 10.0 and 1.6 $\rm \mathring{A}$ and with intensities of 69 CpS and 30 CpS. This mineral is formed due to

the reaction between sulfate in aggregates and cement compounds and causes swelling, expansion and thus reduces the durability of concrete. Ettringite, like C–S–H and unlike Portlandite, does not regenerate during heat application. Peaks such as ettringite were completely omitted at 500 and 900°C. Ettringite is stable up to 105°C and degrades with increasing temperature [52].

At 2.2 Å, the peak related to the quartz mineral is observed with an intensity of 78 CpS, and by applying a temperature of 500°C, the intensity of this peak has decreased by 21% to 61 CpS. At 900°C, another polymorph of silica called tridymite (T) is formed by changing the quartz phase. At 1 atm pressure and at 573°C, α -quartz (low quartz or low-temperature quartz) is converted to β -quartz (high quartz or high-temperature quartz). β -quartz is structurally similar to α -quartz, although there is some distortion in the β -quartz structure [56]. This process is reversible up to 800°C, and the quartz particles are converted to α -quartz by releasing heat and withstanding tensile stresses, creating a void in the concrete. Quartz grains

increase in volume and micro-cracks appear, and the mechanical properties of concrete change [57,58].

In summary, at 25°C, the predominant phases of concrete are C–S–H nanostructure and Portlandite. With increase in the temperature to 500°C, the crystal structures of calcite and quartz form the dominant phase, and a large part of the primary Portlandite and C–S–H nanostructure has been dehydrated and destroyed. With increase in the temperature to 900°C, the concrete matrix consists of cementitious compounds of alite, belite, quicklime (due to primary Portlandite degradation and calcite decomposition), and secondary Portlandite.

3.2 Morphological examination of specimens exposed to heat

Figure 3 shows the SEM images of 28-days-old specimens exposed to different temperatures. Based on the presented images, microcracks, holes, Portlandite (CH) structures,

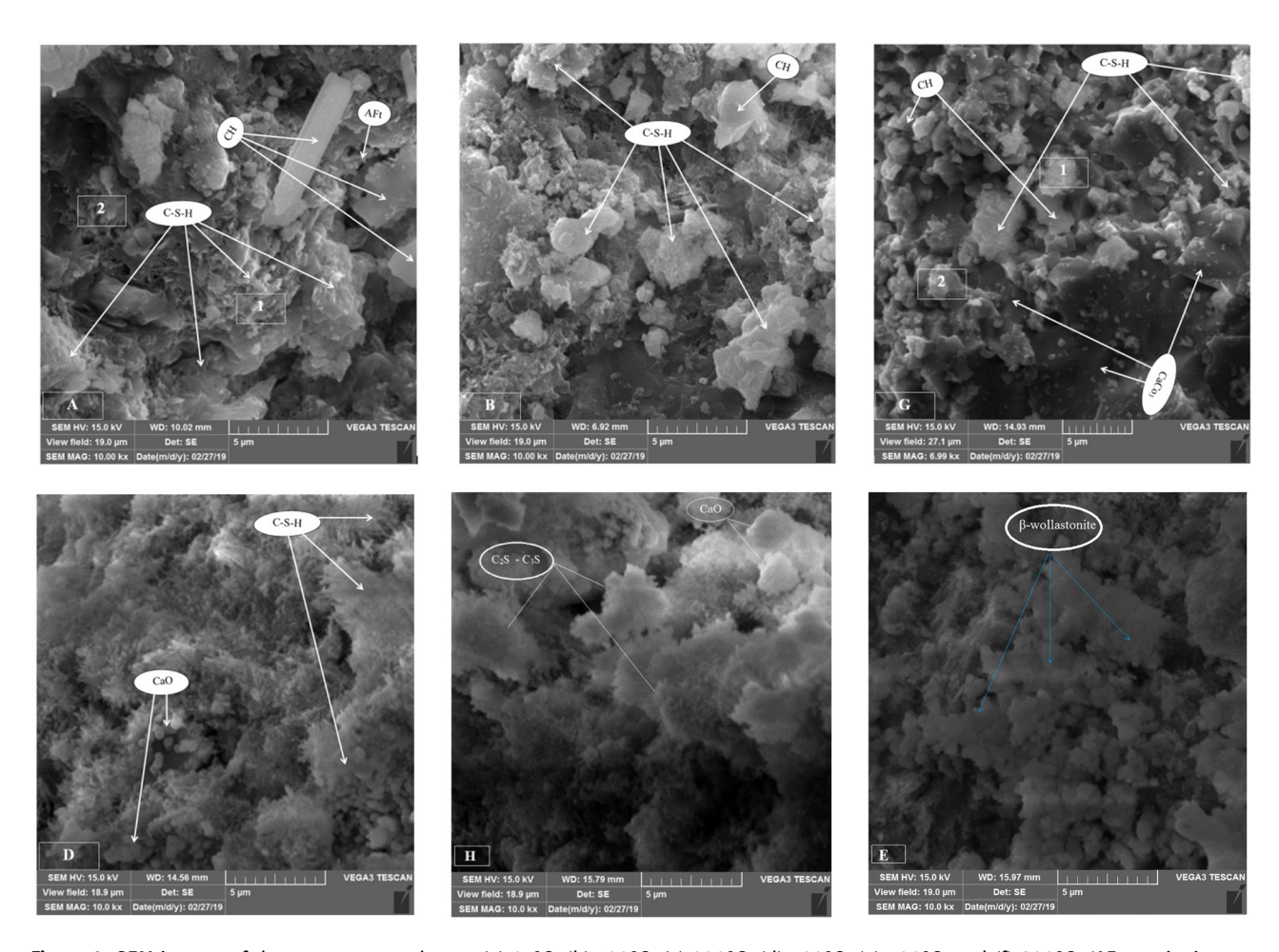


Figure 3: SEM images of the concrete samples at: (a) 25°C, (b) 100°C, (c) 300°C, (d) 500°C, (e) 700°C, and (f) 900°C. (AFt: ettringite, C_3S : alite, C_2S : belite, C_3S : belite, C_3S : calcium silicate hydrate, CH: Portlandite, Q: quartz, Ca: calcite, CaO: Calcium oxide, β-W: β-wollastonite, T: tridymite).

C–S–H nanostructures, and alumina ferric oxide tri-sulfate (AFt) can be distinguished.

In Figure 3a, the SEM image of the sample at 25°C is shown. In this image, calcium hydroxide (Ca(OH₂)) crystals are recognizable as the hexagonal structure, calcium silicate hydrate (C–S–H) as the porous nanostructure, and ettringite as the needle-shaped structure [59,60]. Given that the specimen was at 25°C, no visible cracking is observed at the sample surface, and there are no defects in the concrete surface. The C–S–H nanostructure is also abundantly found in the image. The growth of this nanostructure over time and the hydration process evolution is such that it covers small holes and cracks. Based on EDX analysis, the Ca/Si ratios at points 1 and 2 of Figure 3a are 1.98 and 2.02%, respectively.

Figure 3b shows an image of the sample subjected to 100°C. Removing the surface water of samples made the C–S–H nanostructure and the Portlandite crystals more clearly visible. After removing the surface water of the samples, the C–S–H nanostructure became larger, and the size of this sponge structure increased. At this temperature, the structures of alumina ferric oxide monosulfate (AFm²) and AFt are also destroyed. It is noteworthy that no cracking was observed on the surfaces of these samples. Based on the images and the XRD analysis results, no changes were observed in the cement phases and C–S–H nanostructures up to 200°C.

According to Figure 3c and e, several chemical and physical changes have occurred between 300 and 900°C in the cement paste. Figure 3c is an image of the sample heated at 300°C. The Portlandite and C–S–H nanostructures are still visible. However, compared to the control sample, these structures are declining. The structural changes in these phases also start at 300°C. Due to the complete decomposition of free water and water adsorbed by the concrete, the microcracks begin to expand at 300°C.

Figure 3d shows the SEM image of the sample treated at a temperature of 500°C. It is observed that the Portlandite structure and the C–S–H nanostructure are deteriorating and deforming. According to equation (1), the Portlandite phase is converted to water vapor and calcium oxide as the temperature increases. Portlandite sharply diminishes but does not fall to zero value in cement pastes that were exposed to fire at 600–750°C due to the partial rehydration of lime. The percentage of calcium hydrates was lowered to half its value with rise in the temperature up to 500°C. A severe and complete loss of calcium

Figure 3e shows that the C–S–H nanostructure and Portlandite have been decomposed at 700°C. Calcium carbonate is also converted to lime and carbon dioxide at the temperature range of 730–780°C (according to equation [2]).

$$CaCo_3 + Temperature \rightarrow CaO + CO_2$$
. (2)

Finally, at 900°C, the Portlandite structure and the C–S–H nanostructure are completely decomposed and degraded (Figure 3f). In addition, with the complete decomposition of water from C–S–H nanostructures, it is observed that this structure has been transformed into porous β -W. It is worth noting that this structure affected by high temperatures has changed to a glassy phase. Due to the ceramic structure, heating at 900°C increases porosity, which possibly reduces concrete strength. In general, heating in the temperature range of 500–900°C severely damaged the cement paste structure due to the decomposition of C–S–H nanostructures and the conversion of calcium carbonate (CaCO₃) to CaO and CO₂, and increased cracking.

3.3 Study of compressive strength changes

Figure 4 shows the compressive strength diagrams of concrete samples at temperatures of 25–900°C. The compressive strengths of the 3- and 28-days-old specimens

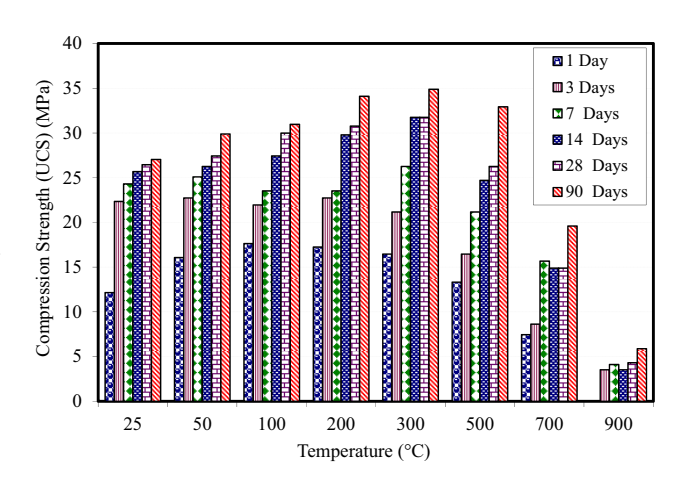


Figure 4: Changes in compressive strength at different temperatures (25–900°C) with curing periods of 1–90 days.

hydrate contents occurred when cement paste was subjected to 600 and 700°C, respectively. This confirms that the dehydration of calcium hydrates is a multi-step reaction because of its complex structure [61] and occurs over a wide range of temperatures (i.e., from 105 to 1,000°C) [62,63].

² Alumina ferric oxide mono-sulfate.

kept at ambient temperature were 18.24 and 26.47 MPa, respectively. According to Figure 3a, due to the C–S–H nanostructure expansion, the specimens' compressive strength increases with aging. The 28 days curing has the highest percentage of C–S–H nanostructures, leading to increased compressive strength. Owing to evaporation, the compressive strength of the 28-days-old specimen at 50°C reached 27.45 MPa (equal to 3.7% increase).

By elevating the temperature up to 200°C, the compressive strength of the specimens increased. As a case in point, in 3- and 28-days-old samples treated at 100°C, the compressive strengths increased to 21.96 and 30.3 MPa, respectively (about 25% increase) due to chemical and physical modifications [64]. At 110°C, the available water existing in the concrete evaporates completely, causing the compressive strength of the dried concrete specimens to increase compared to the saturated ones. The lower resistance in the saturated concrete is due to the separating pressure in the cement paste. Moisture increases the pores' pressure and decreases strength. Another factor contributing to the increase in compressive strength is the removal of the inferior ettringite structure (Figure 3b).

By increasing the temperature to 300°C, the compressive strength of the 3- and 28-days-old samples reached 21.18 and 30.89 MPa, respectively. Due to the loss of water available within the interlayer chemical bonds of C–S–H nanostructural hydrates and sulfoaluminates, the compressive strength begins to decrease at 300°C. Also, according to Figure 3c, it was observed that the C–S–H nanostructure is decomposing, and thus the water in the chemical bonds of this structure will be removed. When cement paste is exposed to heat, hydrated products (calcium silicate hydrate, calcium hydroxide, and calcium sulfoaluminate hydrate) gradually lose their water, and water vapor is generated.

Also, the pressure of concretes' pores increases [65]. This phenomenon starts at about 100°C and continues to about 500°C, which is related to water evaporation temperature from the capillary pores [66]. This process directly affects the concrete strength so that the compressive strength of the 28-days-old sample decreased to 24.71 MPa at 500°C. Considering the SEM images and the results of XRD analysis (Figures 2 and 3f), this decrease in compressive strength is due to the C–S–H nanostructure decomposition. C–S–H nanostructures' intensity is reduced by about 40% at 500°C, implying the decomposition of water chemical bonds and reduction of concrete compressive strength. Furthermore, Portlandite is rapidly decomposed during cooling (reaching ambient temperature) [17,23].

At 700°C, 3- and 28-days-old samples' compressive strengths were 8.62 and 14.9 MPa, 52.6 and 43.7% less

than the control sample, respectively. The decrease in compressive strength at this temperature is due to the decomposition of calcium carbonate into calcium oxide. Moreover, according to Figure 3e, the C–S–H nanostructure is decomposed, and the compressive strength is reduced due to the great microstructural changes. This drop-in compressive strength is more pronounced at 900°C. The 1-day-old sample lost its compressive strength due to its weak structure and incomplete formation of hydration products, including C–S–H nanostructure at the highest temperature (900°C).

Obviously, with increasing age, the specimens have obtained more resistance under thermal conditions. The compressive strengths of 3- and 28-days-old samples at 900°C were 3.53 and 4.31 MPa, respectively. In fact, the decomposition of the C–S–H nanostructure at 900°C, which is also visible in the SEM images (Figure 3f), is the main reason for this sharp drop in strength. In general, the high-temperature decomposition of concrete microstructures, including the conversion of C–S–H nanostructures to unstable glass structures, leads to the reduced strength of the concrete.

3.4 Weight changes in samples affected by heating

Figure 5 shows the weight loss diagram of the cement sample under the influence of heat. The percentage of weight loss of samples held at ambient temperature is zero. As the temperature increases, the specimens' weight loss begins so that at 100°C, 1- and 28-days-old samples had the highest and lowest weight loss with values of 5.86 and 1.66%, respectively. The reason for this weight loss at

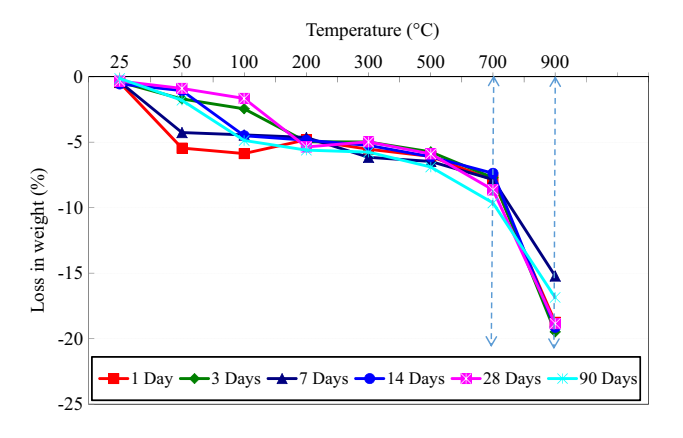


Figure 5: The loss in weight curve of the concrete vs the applied high temperature $(25-900^{\circ}C)$.

a specific temperature of about 100°C is that the inner water of the concrete begins to release and vaporizes at about 120°C. Ettringite also begins to decompose at 100°C. As the temperature rises above 300°C, the weight loss rate of the specimens intensifies. Weight loss percentages of 1- and 28-days-old samples were 5.5 and 4.9%, respectively.

Regarding the weight loss diagram, the slope was mild up to 700°C, but a sharp drop has been observed after that. The reason for this weight loss can be divided into three categories.

There is a slight drop of about 5% in weight loss in the temperature range of 25–150°C. In the temperature range of 150–300°C, an average weight loss of about 6.5% and in the temperature range of 300–700°C, a rapid weight loss of about 9% occur. The main cause of the concrete's physical and chemical changes in the temperature range of 150–300°C is the removal of water from the C–S–H nanostructure. The attenuation of the C–S–H nanostructure is visible in the SEM images. Also, further weight loss in this temperature range is related to the outflow of concrete's inner water from the C–S–H nanostructure hydrates.

In the temperature range above 300°C, concrete loses about 65–80% of its total water volume. Typically, water in the concrete is in various forms, including free water (capillary), absorbed water, and the water in the chemical bonds [67], gradually vaporizing, leading to concrete weight loss.

Based on Figure 5, the weight losses of the 28-daysold sample are 5.89, 8.72, and 18.84%. The maximum weight change at 900°C was about 19%. Weight loss of concrete under high temperatures can be related to changes in the mechanical properties of the concrete. According to the results of SEM images (Figure 3), the samples' weight changes are also affected by the decomposition of C-S-H nanostructures during the heating process.

Due to the presence of all hydration products (including Portlandite, ettringite, monosulfate aluminate, and C–S–H), no weight change is observed in Figure 3a. However, with increase in the temperature to 100°C (Figure 3b), due to the elimination of the ettringite and monosulfate aluminate structures, slight weight changes were observed in Figure 5. According to the SEM results in Figure 3c and d, with increase in the temperature and the onset of the Portlandite structure deformation (initiation of decomposition) and the decrease in the C–S–H nanostructure at the temperature range of 300–500°C, many weight changes have taken place following Figure 5. Finally, according to Figure 3f, all the cement paste structures, particularly the C–S–H nanostructure, have been decayed and destroyed, and that is why at 900°C there is a

sharp weight loss (Figure 5). The results show that water evaporation from the C–S–H nanostructure is responsible for the weight loss in the concrete.

Furthermore, weight loss in concrete depends on the water to cement ratio and the type of aggregates. Water exists in the C–S–H nanostructure between the two layers in the form of $\rm H_2O$ or OH–. Concrete water molecules on the surface can evaporate. Finally, the narrow pores (10–50 nm in the hydrated paste and 3–5 μ m in early ages) between the C–S–H clusters can contain free water [68]. The initial loss might be due to insufficient drying. However, from 80°C onwards, the cause of weight loss is due to water evaporation from the C–S–H structure. Equation (3) estimates the H/S ratio in the C–S–H structure's chemical bonds [69].

$$W_{\text{C-S-H}} = W_{\text{Tot}} - W_{\text{CH}} - W_{\text{Aft}} - W_{\text{Afm}} - W_{\text{cal}}.$$
 (3)

In this equation, W_{Tot} is the overall weight loss from 25 to 900°C. The weight losses due to water evaporation from the Portlandite, ettringite, and monosulfate aluminate structures are shown by W_{CH} , W_{Aft} , and W_{Afm} , respectively. $W_{\rm cal}$ weight loss is also related to calcium carbonate. Weight loss at 50-300°C is due to the lack of hydration in the C-S-H, Aft, and AFm phases. Weight loss at 300-500°C is caused by the water withdrawal from calcium hydroxide (W_{CH}). Carbonation loss is also the cause of weight loss at 600-780°C [69]. In fact, at this temperature, the structure of the Portlandite is completely decomposed. In the range of 500–900°C, all of the weight loss is related to the C-S-H nanostructure. In general, based on the presented results, increase in the temperature exacerbates the weight loss of the concrete specimens.

3.5 Investigation of longitudinal changes in samples exposed to high temperature

The longitudinal variations in the cement samples under the influence of temperature are summarized in Figure 6. Concrete specimens stored at ambient temperature showed insignificant longitudinal changes. During the heating process, from 50 to 500°C, most of the samples experienced a drop in their length so that the 3- and 14-days-old samples at 100°C had 0.1 and 0.65% drop, respectively. The minimum and maximum longitudinal changes in this temperature range were related to these samples. The 14-days-old sample also had a 0.91% weight loss at 300°C. In general, the free water existing in the concrete evaporates at 100–200°C and increases the cement structure's pore pressure.

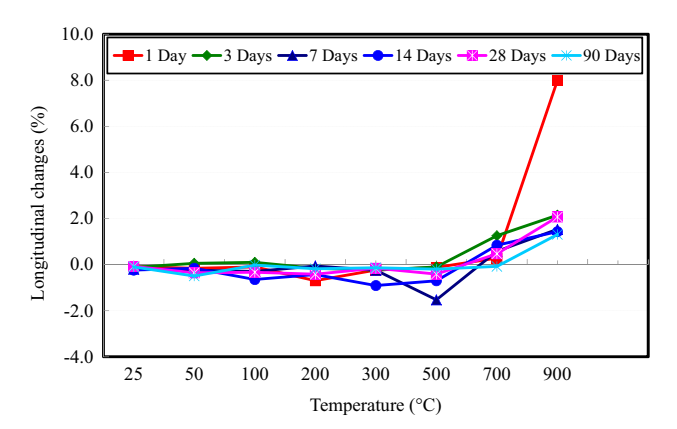


Figure 6: Curve of longitudinal changes of concrete by temperature.

At 300°C, dehydration of calcium hydroxide and C-S-H phase begins (Figure 3c), which leads to the shrinkage and strength decrement of the concrete.

Increasing the temperature up to 500°C resulted in a 1.53% longitudinal drop in the 7-days-old sample with the maximum shrinkage. However, the 3- and 14-days-old samples showed a longitudinal expansion of 0.1 and 0.7% at this temperature, respectively. Generally, concrete specimen lengths increase when exposed to temperatures in the range of 500–900°C. This phenomenon is more tangible above the 700°C. The lowest and the highest longitudinal variations in the 1-, 3-, 7-, 14-, and

28-days-old samples at 700°C were about 0.28-1.26%. In addition, according to Figure 6, the increasing trend of samples length reaches its maximum at 900°C, so that the 1-, 3-, 14-, and 28-days-old sample at this temperature experienced an increase in their length by about 7.99, 2.15, 1.43, and 2.07%, respectively. A lower rate of changes in the longitudinal expansion with temperature was observed due to aging of the specimens. The Portlandite structure $(Ca(OH)_2)$ is one of the most crucial elements in the cement mortar, which leads to the concrete shrinkage at 300-500°C. The shrinkage in the concrete might be attributed to the decomposition of $CaCO_3$ into CaO and CO_2 , which results in the concrete deterioration through volume change [70].

3.6 Examination of heating effects on the apparent concrete properties

Images of heat-treated concrete samples are presented in Figure 7. By examining the specimens' surface images after exposure to heat, the first thing visible is the increase in the surface cavities, whose number and depth increase with the temperature elevation. Hairy cracks were also observed at 200 and 300°C. Based on the studies, at the temperature range between 150 and 300°C, fine cracks

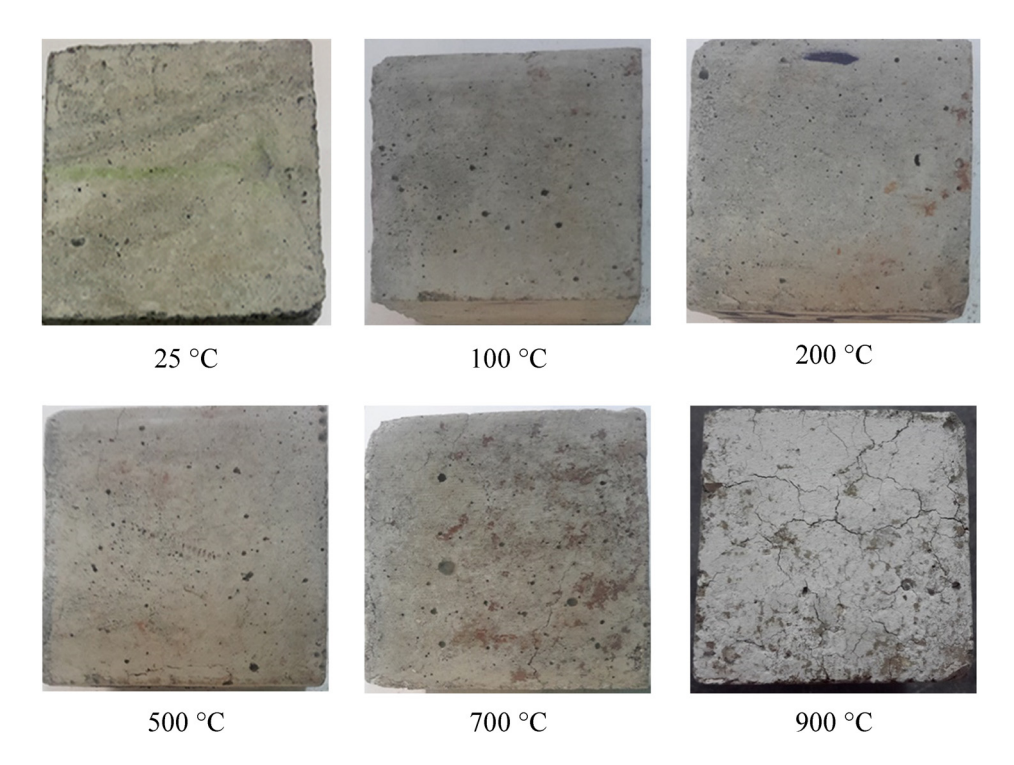


Figure 7: Apparent changes in heated concrete samples.

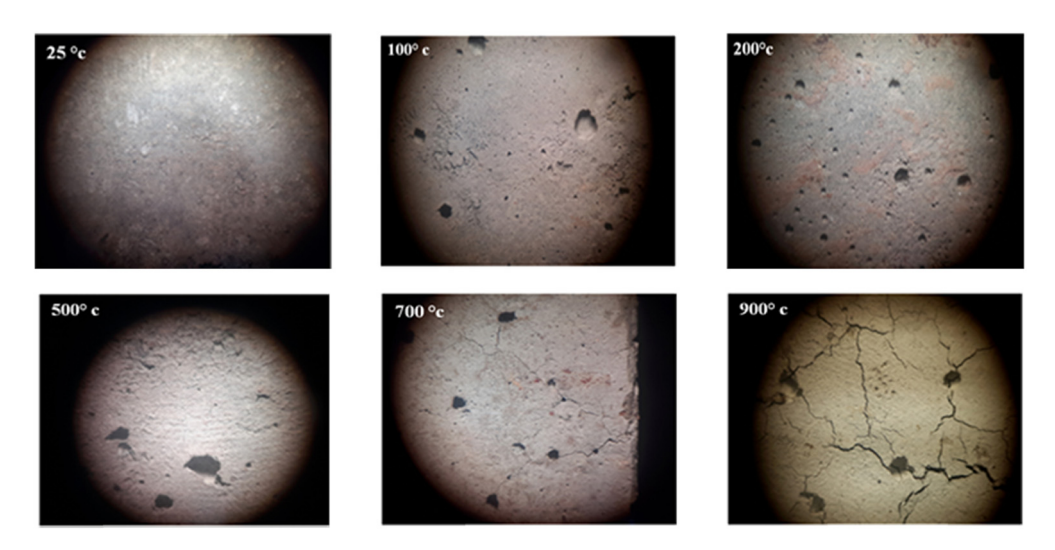


Figure 8: The apparent changes in concrete surface at high temperature.

appeared due to the outflow of water from different hydrates, causing porosity. Also, at temperatures above 300°C, the concrete microstructure (Figure 7) deteriorates, resulting in crystal changes and porosity by above 7% [71]. Thick grid-like deep cracks (about 0.8 mm in width) appeared on the surface of the cement paste that was fired at 700°C. The cracks form as a result of the following factors; (1) the internal pore pressure caused by water vapor that was accumulated after the dehydration of calcium hydrates in case of relatively low permeable cement paste accompanied by loss of mechanical strength, (2) the thermal shock that arises as a result of cooling of the heated cement paste, and (3) the rehydration of lime that is accompanied by a significant increase in volume [72].

Regarding Figure 7, the color change in the samples can be seen with the increase in the temperature from 200°C. Nonetheless, at about 500°C, the sample color turns to light gray. Owing to the loss of the existing chemical and adsorbed water near the solid surface, the color of the specimens is brighter than the control ones to the extent that at high temperatures (around 900°C), the specimens turn to white, and the concrete surface becomes flaky. The reason may be related to the concrete's structural changes since around this temperature, the aggregates in the samples are converted to calcium oxide or lime. The color change of the samples with temperature rise has been studied by Bastami et al., where similar results were obtained [73].

Stereomicroscope images are shown in Figure 8. Examining the surface of the specimens shows that as the temperature increases, the crack growth also intensifies. Also, the color change and the formation of the

cavities are visible. Comparing specimens exposed to high temperatures to those unexposed, it can be seen that with the increase in the temperature, the cracks and cavities increased [4,74].

It should be noted that the starting point for crack growth is from cavities. At 700°C, it is very clear that the micro-cracks started from the cavities and reached inside the cavities at 900°C. So, the entire surface of the sample contains cracks.

4 Conclusion

According to the laboratory studies, the most important results are as follows:

- (a) With increase in the temperature up to 500°C, the intensity of the C-S-H nanostructure's main peak at 3.02 Å decreased from 512 CpS to 331 CpS. The reason for this decrease in peak intensity is the decomposition of water from the chemical structure.
- (b) The C-S-H nanostructure collapses at 900°C, and the β -W ceramic structure is formed.
- (c) Based on the XRD analysis, primary Portlandite is completely degraded at 500°C, and water released at 600°C due to dehydration of Portlandite in reaction with the released lime has led to the formation of secondary Portlandite. As the temperature increases, secondary portlandite increases.
- (d) Examining the samples' compressive strength at 25–200°C showed that as the temperature increases, the strength increases. The lower strength in the

- saturated concrete is due to the separating pressure in the cement paste. In other words, the moisture increases pore pressure and reduces strength.
- (e) Compressive strength is decreased in specimens exposed to high temperature in the range of 500–900°C. The highest decrease in compressive strength was observed at 900°C. The 28-days-old sample at this temperature showed a compressive strength of 4.31 MPa. The drop in compressive strength at this temperature is due to the breaking down of C–S–H nanostructures.
- (f) The higher the temperature, the higher the weight loss. The highest weight loss was observed at 900°C. This is due to the complete decomposition of water from the cement matrix and decomposition of C–S–H nanostructures. The weight loss percentage of 28-days-old sample at this temperature was 18.84%.
- (g) Images of the samples' surfaces show that the color changes at high temperatures in concrete samples. It turns first to gray and subsequently to white. The surface of the specimens also flakes at 900°C.
- (h) These deleterious changes in the concrete samples' composition are accompanied by an increase in the total porosity, severe loss in mechanical strength, and propagation of harmful cracks.

Abbreviations

AFm alumina ferric oxide mono-sulfate
AFt alumina ferric oxide tri-sulfate

ASTM American Society for Testing and Materials

Ca calcite

CH Portlandite: (Ca(OH)₂)
C-S-H calcium silicate hydrate
CpS counts per second

EDS energy-dispersive X-ray analysis

Q quartz

SEM scanning electron microscopy

T tridymite

XRD X-ray diffraction spectroscopy

XRF X-ray fluorescence β -W β -wollastonite

Acknowledgments: The authors of this article would like to thank the University of Hormozgan and Islamic Azad University, Bandar Abbas, for providing some of the materials and equipment for this research.

Funding information: This research was funded by the University of Hormozgan of Iran (2018Y453214).

Author contributions: Mohammad Amiri: conceptualization, methodology, validation, formal analysis, writing – review & editing, supervision. Marzieh Aryanpour: methodology, visualization, writing – review & editing, validation. Fatemeh Porhonar: investigation, resources, investigation, formal analysis.

Conflict of interest: We have no conflict of interest to declare.

Data availability statement: The datasets generated during and/or analyzed during the current study are available from the corresponding author on reasonable request.

References

- [1] Andrushia, A. D., N. Anand, and G. Prince Arulraj. Evaluation of thermal cracks on fire exposed concrete structures using Ripplet transform. *Mathematics and Computers in Simulation*, Vol. 180, 2021, pp. 93–113.
- [2] de Souza, R. C. S., M. Andreini, S. La Mendola, J. Zehfuß, and C. Knaust. Probabilistic thermo-mechanical finite element analysis for the fire resistance of reinforced concrete structures. Fire Safety Journal, Vol. 104, 2019, pp. 22–33.
- [3] Vitorino, H., H. Rodrigues, and C. Couto. Evaluation of postearthquake fire capacity of reinforced concrete elements. *Soil Dynamics and Earthquake Engineering*, Vol. 128, 2020, id. 105900.
- [4] Xing, Q., J. Liao, Z. Chen, and W. Huang. Shear behaviour of fire-damaged reinforced-concrete beams. *Magazine of Concrete Research*, Vol. 72, No. 7, 2020, pp. 357-364.
- [5] Wang, Y., J. Wu, Z. Huang, J. Jiang, G. Yuan, Y. Zhang, et al. Experimental studies on continuous reinforced concrete slabs under single and multi-compartment fires with cooling phase. Fire Safety Journal, Vol. 111, 2020, id. 102915.
- [6] Sadrmomtazi, A., S. H. Gashti, and B. Tahmouresi. Residual strength and microstructure of fiber reinforced self-compacting concrete exposed to high temperatures. *Construction* and Building Materials, Vol. 230, 2020, id. 116969.
- [7] Alizadeh, S. M. M., A. Rezaeian, I. Rasoolan, and B. Tahmouresi. Compressive stress-strain model and residual strength of self-compacting concrete containing recycled ceramic aggregate after exposure to fire. *Journal of Building Engineering*, Vol. 38, 2021, id. 102206.
- [8] Menou, A., G. Mounajed, H. Boussa, C. La Borderie, and A. Saouab. Scaling of thermal damage of cementitious materials: Application to refractory concrete. *High Temperature Materials and Processes*, Vol. 27, No. 3, 2008, pp. 161–174.
- [9] Hertz, K. D. Concrete strength for fire safety design. *Magazine* of Concrete Research, Vol. 57, No. 8, 2005, pp. 445–453.
- [10] Menou, A., G. Mounajed, H. Boussa, C. La Borderie, and K. Lafdi. Thermal damage approach of concrete: Application to specimens subjected to combined compressive and high temperature loads. *High Temperature Materials and Processes*, Vol. 7, No. 1, 2008, pp. 23–40.

- [11] Xu, H., M. Yu, C. Xue, L. Xu, and J. Ye. Experimental study on fire resistance of precast concrete columns with efficient reinforcement. *Engineering Structures*, Vol. 204, 2020, id. 109947.
- [12] Abdulkareem, O. A., A. M. Al Bakri, H. Kamarudin, I. K. Nizar, and A. S. Ala'eddin. Effects of elevated temperatures on the thermal behavior and mechanical performance of fly ash geopolymer paste, mortar and lightweight concrete. *Construction and Building Materials*, Vol. 50, 2014, pp. 377–387.
- [13] Ashkezari, G. D. and M. Razmara. Thermal and mechanical evaluation of ultra-high performance fiber-reinforced concrete and conventional concrete subjected to high temperatures. *Journal of Building Engineering*, Vol. 32, 2020, id. 101621.
- [14] Fernandes, B., A. M. Gil, F. Bolina, and B. F. Tutikian. Microstructure of concrete subjected to elevated temperatures: Physico-chemical changes and analysis techniques. Revista IBRACON de Estruturas e Materiais, Vol. 10, No. 4, 2017, pp. 838–863.
- [15] Kontogeorgos, D. A., G. K. Semitelos, I. D. Mandilaras, and M. A. Founti. Experimental investigation of the fire resistance of multi-layer drywall systems incorporating vacuum insulation panels and phase change materials. *Fire Safety Journal*, Vol. 81, 2016, pp. 8–16.
- [16] Wang, H. The effects of elevated temperature on cement paste containing GGBFS. Cement and Concrete Composites, Vol. 30, No. 10, 2008, pp. 992–999.
- [17] Alonso, C. and L. Fernandez. Dehydration and rehydration processes of cement paste exposed to high temperature environments. *Journal of Materials Science*, Vol. 39, No. 9, 2004, pp. 3015–3024.
- [18] Peng, G. F. and Z. S. Huang. Change in microstructure of hardened cement paste subjected to elevated temperatures. *Construction and Building Materials*, Vol. 22, No. 4, 2008, pp. 593–599.
- [19] Liu, X., G. Ye, G. De Schutter, Y. Yuan, and L. Taerwe. On the mechanism of polypropylene fibres in preventing fire spalling in self-compacting and high-performance cement paste. *Cement* and Concrete Research, Vol. 38, No. 4, 2008, pp. 487–499.
- [20] Saleh, T. A. Nanomaterials: Classification, properties, and environmental toxicities. *Environmental Technology & Innovation*, Vol. 20, 2020, id. 101067.
- [21] Saleh, T. A. A strategy for integrating basic concepts of nanotechnology to enhance undergraduate nano-education: Statistical evaluation of an application study. *Journal of Nano Education*, Vol. 4, No. 1–2, 2013, pp. 1–7.
- [22] Wang, X., W. Ni, J. Li, S. Zhang, M. Hitch, and R. Pascual. Carbonation of steel slag and gypsum for building materials and associated reaction mechanisms. *Cement and Concrete Research*, Vol. 125, 2019, id. 105893.
- [23] Scrivener, K., A. Ouzia, P. Juilland, and A. Kunhi Mohamed. Advances in understanding cement hydration mechanisms. *Cement and Concrete Research*, Vol. 124, 2019, id. 105823.
- [24] Al-Sodani, K. A. A., M. Maslehuddin, O. S. B. Al-Amoudi, T. A. Saleh, and M. Shameem. Performance of corrosion inhibitors in cracked and uncracked silica fume cement concrete beams. European Journal of Environmental and Civil Engineering, Vol. 24, No. 10, 2020, pp. 1573–1588.

- [25] Kunhi Mohamed, A., S. C. Parker, P. Bowen, and S. Galmarini. An atomistic building block description of C-S-H – Towards a realistic C-S-H model. *Cement and Concrete Research*, Vol. 107, 2018, pp. 221–235.
- [26] Jennings, H. M., A model for the microstructure of calcium silicate hydrate in cement paste. *Cement and Concrete Research*, Vol. 30, No. 1, 2000, pp. 101–116.
- [27] Maruyama, I., G. Igarashi, and Y. Nishioka. Bimodal behavior of CSH interpreted from short-term length change and water vapor sorption isotherms of hardened cement paste. *Cement and Concrete Research*, Vol. 73, 2015, pp. 158–168.
- [28] Taylor, H. F. Cement chemistry, London: Thomas Telford, 1997.
- [29] Topcu, I. and A. Demir. Effect of fire and elevated temperatures on reinforced concrete structures. *Bull. Chamber Civil Eng*, Vol. 16, 2002, pp. 34–36.
- [30] Arioz, O. Effects of elevated temperatures on properties of concrete. *Fire Safety Journal*, Vol. 42, No. 8, 2007, pp. 516–522.
- [31] Sakr, K. and E. El-Hakim. Effect of high temperature or fire on heavy weight concrete properties. *Cement and Concrete Research*, Vol. 35, No. 3, 2005, pp. 590-596.
- [32] Savva, A., P. Manita, and K. Sideris. Influence of elevated temperatures on the mechanical properties of blended cement concretes prepared with limestone and siliceous aggregates. *Cement and Concrete Composites*, Vol. 27, No. 2, 2005, pp. 239–248.
- [33] Al-Sodani, K. A. A., M. Maslehuddin, O. S. B. Al-Amoudi, T. A. Saleh, and M. Shameem. Efficiency of generic and proprietary inhibitors in mitigating corrosion of carbon steel in chloride-sulfate environments. *Scientific Reports*, Vol. 8, No. 1, 2018, id. 11443.
- [34] Chen, X., D. Shi, and S. Guo. Experimental study on damage evaluation, pore structure and impact tensile behavior of 10year-old concrete cores after exposure to high temperatures. *International Journal of Concrete Structures and Materials*, Vol. 14, 2020, id. 20.
- [35] Berenjian, J., N. Tila, M. J. Taheri Amiri, and A. Ashrafian. Investigating the effect of high temperatures on long-term compressive strength of self-compacting concrete containing powdery binary admixtures. *Concrete Research*, Vol. 11, No. 1, 2018, pp. 119–128.
- [36] ASTM C136. Standard test method for sieve analysis of fine and coarse aggregates, ASTM International, West Conshohocken, PA. 2006.
- [37] ASTM C566-97. Standard test method for total evaporable moisture content of aggregate by drying, ASTM International, West Conshohocken, PA, 2004.
- [38] ASTM C127-88(2001). Standard test method for density, relative density (specific gravity), and absorption of coarse aggregate, ASTM International, West Conshohocken, PA, 2001.
- [39] ASTM C143/C143M-20. Standard test method for slump of hydraulic-cement concrete, ASTM International, West Conshohocken, PA, 2020.
- [40] ASTM C192/C192M-19. Standard practice for making and curing concrete test specimens in the laboratory, ASTM International, West Conshohocken, PA, 2019.
- [41] Kong, D. L. Y. and J. G. Sanjayan. Effect of elevated temperatures on geopolymer paste, mortar and concrete. *Cement and Concrete Research*, Vol. 40, No. 2, 2010, pp. 334–339.

- [42] ASTM C109/C109M. Standard test method for compressive strength of hydraulic cement mortars (using 2-in. or [50 mm] cube specimens), ASTM International, West Conshohocken, PA, 2021.
- [43] ASTM C31/C31M-21a. Standard practice for making and curing concrete test specimens in the field, ASTM International, West Conshohocken, PA, 2021.
- [44] ASTM C1792-14. Standard test method for measurement of mass loss versus time for one-dimensional drying of saturated concretes, ASTM International, West Conshohocken, PA, 2014.
- [45] ASTM C157/C157M-17. Standard test method for length change of hardened hydraulic-cement mortar and concrete, ASTM International, West Conshohocken, PA, 2017.
- [46] ASTM C39/C39M-21. Standard test method for compressive strength of cylindrical concrete specimens, ASTM International, West Conshohocken, PA, 2021.
- [47] Moore, D. M. and R. C. Reynolds Jr. *X-ray diffraction and the identification and analysis of clay minerals*, Oxford University Press (OUP), Oxford, 1989, pp. 179–201.
- [48] Ouhadi, V. R. and R. Yong. Impact of clay microstructure and mass absorption coefficient on the quantitative mineral identification by XRD analysis. *Applied Clay Science*, Vol. 23, No 1–4, 2003, pp. 141–148.
- [49] Jennings, H. M. Refinements to colloid model of CSH in cement: CM-II. Cement and Concrete Research, Vol. 38, No. 3, 2008, pp. 275–289.
- [50] Sabeur, H., G. Platret, and J. Vincent. Composition and microstructural changes in an aged cement pastes upon two heating-cooling regimes, as studied by thermal analysis and X-ray diffraction. *Journal of Thermal Analysis and Calorimetry*, Vol. 126, No. 3, 2016, pp. 1023–1043.
- [51] Tantawy, M. Effect of high temperatures on the microstructure of cement paste. *Journal of Materials Science and Chemical Engineering*, Vol. 5, No. 11, 2017 id. 80385.
- [52] Rodriguez, E. T., K. Garbev, D. Merz, L. Black, and I. G. Richardson. Thermal stability of CSH phases and applicability of Richardson and Groves' and Richardson C-(A)-SH (I) models to synthetic CSH. Cement and Concrete Research, Vol. 93, 2017, pp. 45–56.
- [53] Rodriguez-Navarro, C., E. Ruiz-Agudo, A. Luque, A. B. Rodriguez-Navarro, and M. Ortega-Huertas. Thermal decomposition of calcite: Mechanisms of formation and textural evolution of CaO nanocrystals. *American Mineralogist*, Vol. 94, No. 4, 2009, pp. 578–593.
- [54] Bodnarova, L., J. Valek, L. Sitek, and J. Foldyna. Effect of high temperatures on cement composite materials in concrete structures. Acta Geodynamica Et Geomaterialia, Vol. 10, No. 2, 2013, pp. 173–180.
- [55] Heikal, M. Effect of temperature on the structure and strength properties of cement pastes containing fly ash alone or in combination with limestone. *Ceramics Silikaty*, Vol. 50, No. 3, 2006, pp. 167–177.
- [56] Ringdalen, E. Changes in quartz during heating and the possible effects on Si production. *Jom*, Vol. 67, No. 2, 2015, pp. 484–492.
- [57] Pabst, W. and E. Gregorová. Elastic properties of silica polymorphs—a review. *Ceramics-Silikaty*, Vol. 57, No. 3, 2013, pp. 167–184.

- [58] Štubňa, I., T. Húlan, T. Kaljuvee, and L. Vozár. Investigation of dynamic mechanical properties of Estonian clay Arumetsa during firing. Applied Clay Science, Vol. 153, 2018, pp. 23–28.
- [59] Taylor, P. C, S. H. Kosmatka, and G. F. Voigt. Integrated materials and construction practices for concrete pavement: A state-of-the-practice manual, United States, Federal Highway Administration. Office of Pavement Technology, 2006.
- [60] Saleh, T. A. Protocols for synthesis of nanomaterials, polymers, and green materials as adsorbents for water treatment technologies. *Environmental Technology & Innovation*, Vol. 24, 2021, id. 101821.
- [61] Zhang, Q. and G. Ye. Dehydration kinetics of Portland cement paste at high temperature. *Journal of Thermal Analysis and Calorimetry*, Vol. 110, No. 1, 2012, pp. 153-158.
- [62] Tantawy, M., A. El-Roudi, E. M. Abdalla, and M. Abdelzaher, Fire resistance of sewage sludge ash blended cement pastes. *Journal of Engineering*, Vol. 2013, 2013, id. 361582.
- [63] Khoury, G., C. Majorana, F. Pesavento, and B. Schrefler, Modelling of heated concrete. *Magazine of Concrete Research*, Vol. 54, No. 2, 2002, pp. 77–101.
- [64] Crozier, D. A. and J. G. Sanjayan. Chemical and physical degradation of concrete at elevated temperatures. *Concrete in Australia*, Vol. 25, No. 1, 1999, pp. 18-20.
- [65] Varona, F., F. J. Baeza, D. Bru, and S. Ivorra. Influence of high temperature on the mechanical properties of hybrid fibre reinforced normal and high strength concrete. *Construction and Building Materials*, Vol. 159, 2018, pp. 73–82.
- [66] Alarcon-Ruiz, L., G. Platret, E. Massieu, and A. Ehrlacher. The use of thermal analysis in assessing the effect of temperature on a cement paste. *Cement and Concrete research*, Vol. 35, No. 3, 2005, pp. 609-613.
- [67] Maanser, A., A. Benouis, and N. Ferhoune. Effect of high temperature on strength and mass loss of admixtured concretes. *Construction and Building Materials*, Vol. 166, 2018, pp. 916–921.
- [68] Beaudoin, J. J., V. S. Ramachandran, and R. F. Feldman. Interaction of chloride and C-S-H. Cement and Concrete Research, Vol. 20, No. 6, 1990, pp. 875-883.
- [69] Gallucci, E., X. Zhang, and K. Scrivener. Effect of temperature on the microstructure of calcium silicate hydrate (C-S-H). Cement and Concrete Research, Vol. 53, 2013, pp. 185-195.
- [70] Yüzer, N., F. Aköz, and L. D. Öztürk. Compressive strengthcolor change relation in mortars at high temperature. *Cement and Concrete Research*, Vol. 34, No. 10, 2004, pp. 1803–1807.
- [71] Fares, H., S. Remond, A. Noumowe, and A. Cousture. High temperature behaviour of self-consolidating concrete: Microstructure and physicochemical properties. *Cement and Concrete Research*, Vol. 40, No. 3, 2010, pp. 488-496.
- [72] Petzold, A. and M. Röhrs. Concrete for high temperatures by Armin Petzold and Manfred Röhrs; Translated [from the German] by AB Phillips and FH Turner, Maclaren, Published by Elsevier Science Ltd, 1970.
- [73] Bastami, M., A. Chaboki-Khiabani, M. Baghbadrani, and M. Kordi. Performance of high strength concretes at elevated temperatures. *Scientia Iranica*, Vol. 18, No. 5, 2011, pp. 1028–1036.
- [74] Alimrani, N. S. and G. L. Balazs. Effect of steel fibres on concrete at different temperatures in terms of shear failure. *Magazine of Concrete Research*, Vol. 73, No. 21, 2021, pp. 1113–1124.